Journal of Materials Chemistry B

ROYAL SOCIETY OF CHEMISTRY

PAPER

View Article Online
View Journal | View Issue

Cite this: J. Mater. Chem. B, 2024, 12, 1826

Effective design of PEGylated polyion complex (PIC) nanoparticles for enhancing PIC internalisation in cells utilising block copolymer combinations with mismatched ionic chain lengths†

Fadlina Aulia,[a] Hiroaki Matsuba,[a] Shoya Adachi,[a] Takumi Yamada,[a] Ikuhiko Nakase,[g] Teruki Nii,[b] Takeshi Mori,[bc] Yoshiki Katayama[bcdef] and Akihiro Kishimura[*bcd]

In nanomedicine, PEGylation of nanomaterials poses a dilemma since it inhibits their interaction with target cells and enables their retention in target tissues despite its biocompatibility and nonspecific internalisation suppression. PEGylated polypeptide-based polyion complexes (PICs) are fabricated *via* the self-assembly of PEGylated aniomers and homocatiomers based on electrostatic interactions. We propose that various parameters like block copolymer design and PIC domain characteristics can enhance the cell–PEGylated PIC interactions. Remarkably, the properties of the PIC domain were tuned by the matched/mismatched ionomer chain lengths, PIC domain crosslinking degree, chemical modification of cationic species after crosslinking, PIC morphologies (vesicles/micelles) and polyethylene glycol (PEG) chain lengths. Cellular internalisation of the prepared PICs was evaluated using HeLa cells. Consequently, mismatched ionomer chain lengths and vesicle morphology enhanced cell–PIC interactions, and the states of ion pairing, particularly cationic residues, affected the internalisation behaviours of PICs *via* acetylation or guanidinylation of amino groups on catiomers. This treatment attenuated the cell–PIC interactions, possibly because of reduced interaction of PICs with negatively charged species on the cell-surface, glycosaminoglycans. Moreover, morphology and PEG length were correlated with PIC internalisation, in which PICs with longer and denser PEG were internalised less effectively. Cell line dependency was tested using RAW 264.7 macrophage cells; PIC recognition could be maintained after capping amino groups on catiomers, indicating that the remaining anionic groups were still effectively recognised by the scavenger receptors of macrophages. Our strategy for tuning the physicochemical properties of the PEGylated PIC nanocarriers is promising for overcoming the PEG issue.

Received 4th September 2023,
Accepted 18th January 2024

DOI: 10.1039/d3tb02049e

rsc.li/materials-b

Introduction

The introduction of polyethylene glycol (PEG) into a polymer or the surface of nanomaterials, termed PEGylation, has become a gold standard to enhance the biocompatibility, anti-fouling activity, and colloidal stability of such materials as well as to reduce their immunogenicity and possibility of enzyme digestion.[1] PEGylation can prolong the blood retention time of nanomaterials and promote their accumulation in tumour sites *via* the enhanced permeability and retention (EPR) effect. The effect of prolonged circulation can be achieved by reducing cell interaction, as reported for several PEGylated nanoparticles, PEGylated liposomes, and several inorganic-sourced nanoparticles, such as iron, silver and gold.[2,3] However, biomacromolecular drugs, such as nucleic acids and proteins, must be delivered inside the target cells to show their therapeutic effects.

[a] Graduate School of Systems Life Sciences, Kyushu University, 744 Moto-oka, Nishi-ku, Fukuoka 819-0395, Japan
[b] Department of Applied Chemistry, Faculty of Engineering, Kyushu University, 744 Moto-oka, Nishi-ku, Fukuoka 819-0395, Japan. E-mail: kishimura.akihiro.776@m.kyushu-u.ac.jp
[c] Center for Future Chemistry, Kyushu University, 744 Moto-oka, Nishi-ku, Fukuoka 819-0395, Japan
[d] Center for Molecular Systems, Kyushu University, 744 Moto-oka, Nishi-ku, Fukuoka 819-0395, Japan
[e] Center for Advanced Medical Open Innovation, Kyushu University, 744 Moto-oka, Nishi-ku, Fukuoka 819-0395, Japan
[f] Department of Biomedical Engineering, Chung Yuan Christian University, 200 Chung Pei Rd., Chung Li, Taiwan, 32023, ROC
[g] Department of Biological Chemistry, Graduate School of Science, Osaka Metropolitan University, 1-1, Gakuen-cho, Naka-ku, Sakai-shi, Osaka 599-8531, Japan

† Electronic supplementary information (ESI) available. See DOI: https://doi.org/10.1039/d3tb02049e

Based on an *in vitro* study reported by Mishra *et al.*,[4] PEGylation of polycation–plasmid DNA complexes suppressed their cellular uptake and then reduced their protein expression to less than half of that of the non-PEGylated variants. Several solutions have been suggested to overcome these problems, such as installing targeting ligands on the PEG surface to enhance cellular uptake and environmentally responsive cleavable PEGylation.[5,6] However, to realise a more versatile and facile application of PEGylated nanocarriers, the correlation between their physicochemical properties and cellular internalisation must be clarified in the presence of PEG without cumbersome modifications. In other words, the cellular internalisation of nanocarriers without PEG detachment or ligand introduction should provide insights into an effective design strategy to overcome the PEG dilemma. Oh *et al.* discussed how the PEGylated gold nanoparticle size affected its cellular uptake, but in the presence of a peptide ligand.[7] Li *et al.* studied the endocytosis behavior of PEGylated nanocarriers using dissipative particle dynamics (DPD) simulations but from the view point of PEG properties.[8] Pelaz *et al.* investigated the effect of PEG-coated nanoparticles on the cellular uptake from the viewpoint of protein adsorption.[3] As no specific studies discussed the aspect of materials design, particularly the physicochemical nature of nanoparticles themselves, we attempted to focus on tuning the nanocarrier physicochemical properties, followed by PEG characteristics.

Our goal is to identify parameters related to the properties of nanocarriers that can promote their cell internalisation and compromise the impact of PEG on the nanocarriers. To this end, we decided to use PEGylated polyion complexes (PICs), which are prepared from PEGylated polyelectrolytes under aqueous conditions *via* electrostatic complexation, to provide different types of nanoarchitectures designed for drug delivery systems (Scheme 1). The most typical example is the PIC micelle, first reported as an assembly of oppositely charged block copolymers with a PEG segment in an aqueous environment.[9] Since PIC micelles are characterised by their sizes of several tens of nanometres and protective hydrophilic and biocompatible shell and drug-loadable core, they can show prolonged blood circulation time and enhanced permeability and retention (EPR) effect, which are favourable properties for a drug delivery vehicle.[10,11] Many studies reported the successful loading of plasmid DNA, mRNA, oligonucleotides, and proteins into PIC micelles.[10–15] Thus, they can be a promising carrier for developing non-viral gene delivery systems for vaccines and oligonucleotide therapeutics for cancer therapy.[10,15] A relatively new PIC nanoarchitecture is the PICsome, a nanosized unilamellar vesicular PIC with a hollow structure.[16] PICsomes can be prepared from PEGylated polyelectrolytes by tuning the chemical design of PEGylated polymers, such as the PEG fraction[17,18] and charged species,[19,20] which allow effective encapsulation of neutral and charged macromolecules, such as dextran,[21] enzymes,[22,23] and inorganic nanoparticles,[24,25] and incorporate oligonucleotides in their PIC membrane.[26,27] Compared to lipid-based vesicles, PICsomes are featured by their unique semipermeable PIC membrane, which is useful for retaining macromolecular cargoes and transporting small molecular weight compounds, *e.g.*, drugs and substrates for enzymes, across their membrane. Therefore, PICsomes can function *in vivo* as nanoreactors and drug reservoirs.[22,23,28–30] Besides, the PIC domain's physicochemical properties, particularly stability and semipermeability, can be modulated by crosslinking[31,32] and the choice of side chain functionalities of the polyelectrolytes.[28,33] Crosslinked PICsomes show size-dependent disposition into organs and tumour sites *in vivo*.[31] Thus, PICs can provide a promising platform to obtain nanovehicles with systematic design based on a series of chemically tuned components. This platform is helpful for clarifying the correlation between the physicochemical properties of nanocarriers and their ability to interact with cells and further internalisation.

In this study, we demonstrate that fine-tuning the physicochemical properties of PICs is a promising solution for overcoming the PEG dilemma. A series of PEG-based block ionomers were synthesised by varying their charged segment and PEG lengths to fabricate various types of PIC nanoparticles and thus evaluate their internalisation in living cells. To modulate the properties of the PIC domains, combinations of polymers with mismatched ionomer lengths were examined to enhance the cellular internalisation. In addition, the importance of PIC domain crosslinking and its fine-tuning, such as cationic residue modification, which modulates PIC interactions with the cell surface, was revealed. To the best of our knowledge, this study is the first that sought to reveal the correlations between the physicochemical properties of PEGylated PICs and their cellular internalisation. The convenient design and tunable characteristics of PICs might provide key insights into biomaterials development and applications to overcome the PEG dilemma.

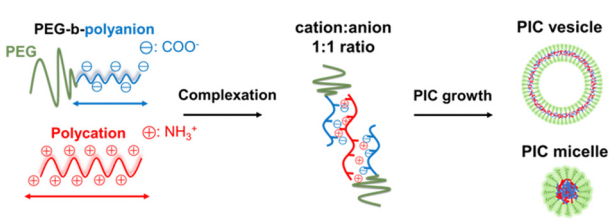

Scheme 1 Illustration of typical PIC nanoarchitecture formation.

Experimental

Materials

β-Benzyl-L-aspartate *N*-carboxy-anhydride (BLA-NCA) and ε-trifluoroacetyl-L-lysine *N*-carboxy-anhydride (L-Lys(TFA)-NCA) were obtained from Chuo Kaseihin Co. Inc. (Tokyo, Japan). α-Methoxy-ω-amino poly(ethylene glycol) (MeO–PEG–NH_2) (number average molecular weight, M_n = 2000, 5000) was purchased from NOF Co. Ltd (Tokyo, Japan) and purified by ion-exchange chromatography using CM Sephadex C-50 from Sigma-Aldrich (Missouri, USA). *n*-Butylamine (special grade) was purchased from Wako Pure Chemical Co., Ltd (Osaka, Japan), refluxed for 3 h, and distilled over CaH_2 at 78 °C under a N_2 atmosphere. Acetonitrile, dimethyl

sulfoxide (DMSO), methanol, n-hexane, chloroform ($CHCl_3$) (super dehydrated), benzene (super dehydrated), dichloromethane (super dehydrated), and *N,N*-dimethylformamide (DMF) (super dehydrated) were also purchased from Wako Pure Chemical Industries and used as received. Di-isopropyl ethyl amine (DIPEA) and deuterium oxide (D_2O) were purchased from Sigma-Aldrich. The Cy3 NHS ester was purchased from LumiProbe (Maryland, OH, USA). 1-Ethyl-3-(3-(dimethylamino)propyl)-carbodiimide hydrochloride (EDC) was purchased from Tokyo Chemical Industry Co., Ltd (Tokyo, Japan). Calcein was purchased from Wako Pure Chemical Co., Ltd. 3,5-Dimethyl-1-guanylpyrazole nitrate (DMGP) was purchased from Sigma-Aldrich. Acetic anhydride and 2,4,6-trinitrobenzenesulphonic acid sodium salt dihydrate were purchased from Wako Pure Chemical Industries, Ltd. Copper grids (150 mesh) coated with a thin Formvar film and reinforced with a carbon coating were purchased from JEOL (Tokyo, Japan).

Methods

Synthesis of aniomers. Poly(α,β-aspartic acid) (PAsp) was synthesised as a PEGylated block copolymer. PEG with M_W = 2000 and 5000 (PEG_{2k} and PEG_{5k}, respectively) were used as PEG blocks. Poly(β-benzyl-L-aspartate) (PBLA) was synthesised *via* ring-opening polymerisation using BLA-NCA as the monomer, as previously reported.[34] MeO–PEG–NH_2 was used as the initiator. PEG-PAsp was obtained *via* the direct hydrolysis of PEG-PBLA according to the method described previously.[35] Briefly, lyophilised PEG-PBLA was dissolved in acetonitrile and then added to 0.5 M NaOH to obtain PEG-PAsp in its Na^+ salt form.

Synthesis of catiomers. Poly-L-lysine (PLL) synthesis was performed as previously reported.[36] PLL was synthesised as a homo- or PEGylated block copolymer. PEG_{2k} and PEG_{5k} were used as the PEG blocks. Briefly, homo–PLL(TFA) and PEG-PLL(TFA) were prepared *via* the ring-opening polymerisation of Lys(TFA)-NCA initiated by 5-butylamine and MeO-PEG-NH_2, respectively. PLL-HCl was obtained by hydrolysing PLL(TFA) under basic conditions using excess NaOH against TFA groups, followed by dialysis against an HCl solution.

Synthesis of fluorophore-labelled polymers. Fluorophore labelling was performed on the terminal –NH_2 group of PAsp. One equiv of Cy3-NHS was added to a 10 mg mL^{-1} polymer solution prepared in 100 mM phosphate buffer (PB, pH 8.0). The mixture was then stirred for 24 h at 25 °C. The polymer was purified *via* dialysis using a Spectra/Por cellulose membrane (molecular weight cut-off (MWCO): 3500, Spectrum Laboratories, California, USA) against ultrapure water (UPW) with more than 7× outer liquid exchanges (the presence of free dye was confirmed by reading Cy3 fluorescence intensity using a plate reader against a blank solution). The resulting solution was lyophilised to obtain a powder. The labelling ratio was determined by UV-vis spectroscopy using a JASCO V-670 spectrophotometer (Jasco International Co., Ltd, Tokyo, Japan) with a calibration curve of Cy3 (ε = 150 000 M^{-1} cm^{-1} at λ = 570 nm). For further particle fabrication, the labelling ratio was adjusted to 10% of the total polyanion chains by mixing with a non-labelled polymer solution.

Determination of the degree of polymerisation (DP). The ^1H NMR spectra of the polymers were recorded using a JNM-ECZ400S instrument (JEOL, Tokyo, Japan) at a frequency of 400 MHz in D_2O at a concentration of 10 mg mL^{-1}. Trimethylsilylpropanoic acid (TMSP) was used as the internal reference (0 ppm). Peak integrations were computed using the Delta software (version 5.0.5.1, JEOL), and the number-averaged DP and molecular weight were calculated. The DP of the Asp segment was determined from the peak area ratio of the PAsp proton (–CH_2COO; δ 2.75; peak c1, c2 in Fig. S1–S4, ESI†) side chains to the methylene protons in PEG (–OCH_2CH_2–; δ 3.70). The DP of the PLL segment was determined from the peak area ratio of protons of the PLL side chains (–CH_2–; δ 3.00; peak d in Fig. S5–S7, ESI†) to the methyl proton of the butyl terminus for homo PLL (–CH_3; δ 0.9; peak f in Fig. S5 and S6, ESI†) and to the methylene protons in PEG for the block copolymer (–OCH_2CH_2–; δ 3.70; peak PEG in Fig. S7, ESI†). The results are summarized in Table 1.

Determination of polymer dispersity (*Đ*). Size exclusion chromatography (SEC) measurements of the synthesised polymers were conducted using a high-performance liquid chromatography (HPLC) system (JASCO International Co., Ltd) equipped with a Superdex 200-10/300GL column (Cytiva, Massachusetts, USA), an interface box (LC-Net II/ADC JASCO International Co., Ltd, Tokyo, Japan), a refractive index detector (RI-4030 JASCO International Co., Ltd, Tokyo, Japan), a UV/vis detector (UV-4075 JASCO International Co., Ltd) and an RHPLC pump (PU-4180 JASCO International Co., Ltd). PB buffer (10 mM, pH 7.4) containing 500 mM NaCl was used as an aqueous eluent at a flow rate of 0.5 mL min^{-1} at 25 °C. *Đ* was computed using a calibration curve from standard PEO of known molecular weights (ReadyCal-Kit PEO/PEG, M_p 232–1015 000; Scharlab, Barcelona, Spain). The results are summarised in Table 1.

Fabrication of PIC nanoparticles. The polymer combinations used to prepare the PICs are listed in Table 2. PICs were prepared based on previous reports with minor modifications.[21] Typically, polycations and polyanions were separately dissolved in 50 mM PB (pH 7.4) at a concentration of 1.0 mg mL^{-1}. The polycation solution was added to the polyanion solution in an equal unit ratio of –COO^- and –NH_3^+ groups (see eqn (S1) for

Table 1 Characterisation of polymers used for PIC formation

Polymer list	DP[a]	*Đ*[b]	MW[c]
PEG_{2k}–PAsp	56	1.02	10 063
	69	1.06	13 527
	93	1.4	15 950
PEG_{5k}–PAsp	70	1.11	14 992
Homo–PLL	64	1.06	10 601
	100	1.6	16 418
PEG_{2k}–PLL	81	1.13	20 482

[a] DP: degree of polymerization. [b] *Đ*: dispersity. [c] MW: molecular weight.

Table 2 PIC polymer combinations and particle characteristics

PIC type	Polyanion (DP)	Polycation (DP)	f_{PEG}[a] (%)	Average diameter (nm)	Polydispersity index (PdI)	ζ-potential (mV)	Crosslinking degree of PICs (%)	Amine modification rate (%)
Vesicle	PEG_{2k}–PAsp(56)	Homo–PLL(100)	10	127	0.03	−1.5		None (N)
				159	0.13	−9.9	50	50 (for acetylation, A)
				106	0.12	−1.8		20 (for guanidinylation, G)
				162	0.08	−0.2	80	—
	PEG_{2k}–PAsp(69)	Homo–PLL(64)	9	180	0.07	−1.8	80	—
	PEG_{2k}–PAsp(93)	Homo–PLL(64)	7	200	0.2	−1.2	80	—
2k-Micelle	PEG_{2k}–PAsp(56)	PEG_{2k}-PLL(81)	14	29	0.03	−2.1	50	—
5k-Micelle	PEG_{5k}–PAsp(70)	homo–PLL(100)	19	42	0.03	−3.6	50	—

[a] f_{PEG}: PEG fraction after complexation, defined by the fraction of PEG in a total PIC. See eqn (S3) in the ESI.

calculation, ESI†). The resulting mixture was pipetted ten times and subjected to the dynamic light scattering (DLS) measurement. Subsequently, crosslinking of the PICs was performed by adding a specific amount of 10 mg mL^{-1} EDC solution (50 mM PB, pH 7.4) to the PIC solutions. The EDC amounts varied in the range between 4 (for the PIC with a crosslinking degree of 50%, 50%-CL PIC) and 10 equiv. (for the PIC with a high crosslinking degree, 80%-CL PIC) with respect to the number of $-COO^-$ groups on the polyanion. Then, the samples were stored at 4 °C for 12 h. Unreacted EDC was removed using a polyethersulphone ultrafiltration membrane (MWCO: 300 000 for vesicles, 100 000 for micelles; VivaSpin 6, Sartorius AG, Gottingen, Germany) by exchanging the solvent with UPW three times at 4 °C using gravity force.

Determination of the crosslinking degree. The degree of crosslinking was determined by quantifying the number of residual amino groups using a trinitro benzenesulphonic acid (TNBS) assay (Scheme S1, ESI†). TNBS was dissolved in DMF containing 10% (v/v) DIPEA, and 25 μL of the solution was added to 1000 μL of 50 mM bicarbonate buffer (pH 8.5). The resulting solution was added to 10 μL of the diluted PIC solution. After 90 min of incubation at 25 °C, absorbance was measured at 420 nm. The amino groups were quantified using a calibration curve obtained from the polycations used for PIC preparation. The degree of crosslinking was calculated using the following equation (see eqn (S2), ESI†).

$$\text{Crosslinking degree [\%]} = 100 - (\text{detected amino groups, \%})$$

AFM measurements. A 1 cm^2 square-shaped cut mica substrate was fixed on a dish and used as the stage for measurement. The top layer of mica was removed by pressing adhesive tape against the surface. Then, 10 μL of crosslinked PIC vesicle solution in the phosphate-buffered saline (pH 7.4) was placed on the mica stage and let stand for 1 min. The mica surface was then carefully washed and soaked in PBS. Wet condition measurements were performed using atomic force microscopy (AFM) (AFM Dimension XR microscope (Bruker, Massachusetts, US)) with a peak force of 150 pN and a frequency of 1 kHz (Cantilever Olympus Biolever BL-AC40 TS-C2k 0.09 N m^{-1}). Area of deformation of PICs was quantified from at least 20 particles taken from several images using ImageJ (U. S. National Institutes of Health, Bethesda, Maryland, USA).

Acetylation and guanidinylation of the cationic residue. For acetylation, 50%-CL PIC particles were treated with excess acetic anhydride (1000 equiv. of free amino groups). After 12 h of reaction, the resulting particles were purified by gravity using an ultrafiltration membrane. For guanidinylation, the solvent containing 50%-CL PIC particles was replaced with a buffer, 500 mM Na_2CO_3 (pH 9.5, adjusted with 1 M HCl) using an ultrafiltration membrane (VivaSpin 6, MWCO: 300 000) by gravity force. A buffer solution of DMGP (40 mg mL^{-1}) was then added to the PIC solution with 50 equiv. of residual amines in the PIC particles. After shaking for 12 h at 40 °C, the resulting mixture was purified by ultrafiltration (VivaSpin 6, MWCO: 300 000) by gravity force using UPW. Thereafter, the modification rate was evaluated using the same method as described in the 'Determination of the crosslinking degree' section by quantifying residual amines.

DLS and ζ-potential measurements. A Zetasizer Pro (Malvern PANalytical, Malvern, UK) equipped with an ion He–Ne laser (λ = 633 nm) at measurement angles of 173° and 13° was used to analyse the size distributions and ζ-potentials of PICs at 25 °C. For ζ-potential measurement, 1 mL of each PIC solution in 10 mM PB buffer of pH 7.4 was introduced into a cuvette (disposable folding capillary cuvette DTS1070, Malvern Panalytical, Malvern, England).

Transmission electron microscopy (TEM). TEM was performed using a JEM-1400 instrument (JEOL, Tokyo, Japan) operated at 120 kV to clarify the morphology of the crosslinked PIC particles. Electron micrographs were captured with a charge-coupled device camera cooled at −20 °C. A 150-mesh copper grid was hydrophilised using an HDT-400 hydrophilic treatment device (JEOL, Tokyo, Japan), and 2 μL of the PIC sample was placed on the grid. After drying for 3 min, 2 μL of Gd acetate solution (2% w/v) was added for staining, and the sample was allowed to dry for an additional 3 min. Any excess solution was carefully removed using a filter paper, and the grids were air-dried at 25 °C.

Cryo-TEM observation. Cryo-TEM observation was performed to verify the inner hollow structure of the PIC. The ultrapure water solution of the PIC (56, 100) with a crosslinking degree of 50% was dropped onto a Quantifoil grid (a copper grid coated with a thin film of R2/1 holey carbon, purchased from EM Japan, Tokyo, Japan). The Quantifoil grid containing the sample solution was

blotted onto a paper to remove excess sample solution on a Leica EM GP plunge freezer (Leica Microsystems, Wetzlar, Germany). The sample solution was immediately vitrified by rapid immersion in liquid ethane (−175 °C). The frozen specimen was transferred to a JEM-2100F instrument (JEOL, Tokyo, Japan) using a cryo-transfer holder (Gatan 914, Gatan, Pleasanton, CA, USA) at liquid nitrogen temperature throughout the measurement. The microscope was equipped with a field emission gun (ZrO/W(100)) and a 4k × 4k CCD camera (UltraScan, Gatan, Pleasanton, CA, USA).

Cell culture. Human cervix carcinoma (HeLa) and mice macrophage (RAW 264.7) cells were cultured in phenol red-containing Dulbecco's modified Eagle medium (DMEM) (Nacalai Tesque Inc., Kyoto, Japan) supplemented with 10% fetal bovine serum (FBS) (GIBCO, Waltham, MA, USA) and 1% antibiotic–antimycotic mixed stock solution 100× (penicillin 10 000 U mL^{-1}, streptomycin 10 000 μg mL^{-1} and amphotericin B 25 μg mL^{-1}) (Nacalai Tesque Inc., Kyoto, Japan). CHO-K1 (wild-type) and CHO-A745 (glycosaminoglycan-deficient cells) were cultured in Ham's F-12K (Kaighn's Modification) (Fujifilm Wako Pure Chemical Corporation, Osaka, Japan) as a basic medium supplemented with 10% FBS and 1% antibiotic–antimycotic mixed stock solution under 5% CO_2 at 37 °C. Human colorectal adenocarcinoma (Caco2) cells were cultured in phenol red-containing DMEM (Nacalai Tesque Inc.) supplemented with 10% FBS (GIBCO), 1% antibiotic–antimycotic mixed stock solution (Nacalai Tesque Inc.) and 1% MEM non-essential amino acid solution (Nacalai Tesque Inc.). Mice dendritic cells (DC 2.4) were cultured in Roswell Park Memorial Institute-1640 (RPMI-1640) medium (Nacalai Tesque Inc.) supplemented with FBS (GIBCO), 1% antibiotic–antimycotic mixed stock solution (Nacalai Tesque Inc.) and 2-mercaptoethanol (final conc. 50 μM) (Fujifilm; Wako Pure Chemical Corporation). Cell passage was performed after suspending the cells for 5 min in enzyme-free cell dissociation solution (Merck, Frankfurt, Germany), followed by centrifugation at 1000 rpm for 3 min to obtain a cell pellet. The cells were resuspended in the cell culture medium, seeded at 2×10^5 cells in 10 mL of the medium on a 10 mm culture dish, and allowed to grow to 80% confluency.

Evaluation of cellular internalisation of PICs by fluorescence imaging. Cells were seeded at 2×10^4 cells per well in a 96-well plate and cultured for 24 h. The cell layers were rinsed twice with 100 μL of DPBS to completely remove the culture medium. To 90 μL of the culture medium, 10 μL of the PIC solution was added (the final concentration of PAsp = 0.02 mg mL^{-1}). Cells were incubated at 37 °C and 5% CO_2 for a designated period. After incubation, cells were rinsed with DPBS twice and were fixed with 4% paraformaldehyde in PBS (Nacalai Tesque Inc.) by 10-min incubation. Nuclear staining was performed using Hoechst 33342 solution (1000-fold diluted in the culture medium) by 3 min of incubation, followed by washing with 100 μL of DPBS twice. Microscopic imaging was performed using a confocal laser scanning microscope (CLSM, LSM700 AxioObserver; Carl Zeiss, Oberkochen, Germany) equipped with a Plan-Apochromat 63×/1.40 Oil DIC M27 objective lens and a photomultiplier tube detector.

Line profiling analysis of HeLa cells. Line profiling was performed to investigate the subcellular distribution of PICs using a ZEISS ZEN 3.8 (ZEN lite, Carl Zeiss, Oberkochen, Germany). A scan line was drawn over the cell to cover the membrane, nucleus, and PICs. The intensity of each fluorescence signal was obtained from the "Profile" submenu.

Quantification of PIC cellular uptake by flow cytometry (FCM). Cells were seeded at 2×10^5 cells per well in a 6-well plate and cultured for 24 h. The cell layers were rinsed twice with 1000 μL of DPBS to completely remove the culture medium. To 900 μL of the culture medium, 100 μL of the PIC solution was added (the final concentration of PAsp = 0.02 mg mL^{-1}). Cells were incubated at 37 °C and 5% CO_2 for a designated period. The internalisation of PICs into cells was quantified by FCM. Briefly, suspended cells obtained after 5 min of treatment with an enzyme-free cell dissociation solution (Merck) were subjected to centrifugation at 1000 rpm at 4 °C for 3 min to obtain a cell pellet. The resulting cell pellet was redispersed in the culture medium, and the cells were analysed using a Cytoflex S flow cytometer (Beckman Coulter, Indianapolis, United States) equipped with a 561 nm laser. In the quantification results, fluorescence intensities were normalised in the way indicated in each figure legend.

Cytotoxicity assay. Cytotoxicity against HeLa cells was assessed using a Cell Counting Kit-8 (CCK-8) viability kit (Dojindo Molecular Technologies, Inc., Kumamoto, Japan). Briefly, the cells were cultured in the appropriate medium as mentioned above. After reaching confluence, the cells were seeded in a 96-well plate at a concentration of 2×10^4 cells per well and incubated for 24 h at 37 °C and 5% CO_2. The following day, the cells were treated with all of the samples separately and further incubated for 24 h at 37 °C under 5% CO_2. CCK-8 was added to all test wells according to the manufacturer's instructions and incubated for 2 h at 37 °C under 5% CO_2. Absorbance was measured at 450 nm using an Infinite 200 PRO Tecan plate reader (Männedorf, Switzerland).

Statistical analysis. Data are presented as means ± standard deviation. Statistical analyses were conducted using Student's *t*-test (*t*-test) to compare the values of two groups. Data were analysed using Microsoft Excel office 2019 at $*p < 0.05$, $**p < 0.01$, and $***p < 0.001$, and the differences were regarded as having statistical significance.

Results and discussion

Polymer synthesis and characterisation

Polypeptide-based materials have been generally used for polyelectrolyte complexation because of their feasible polymerisation and stable secondary and tertiary structures.[37] A combination of carboxyl groups from PAsp as an anion source and amine groups from PLL as a cation source was selected because both ionic residues exhibited high ionisation rates at neutral pH.[38] Catiomers and aniomers were prepared as homo- and block copolymers using PEGs with different molecular weights of 2000 (PEG_{2k}) and 5000 (PEG_{5k}). The DP was designed to be between 60 and 100

repeating units for homo- and PEG-block copolymers. The DP was determined by NMR spectroscopy, and $Đ$ of the polymers was determined by SEC (Table 1 and Fig. S1–S7 (NMR) and Fig. S9–S15 (SEC) in the ESI†).

PIC fabrication and characterisation

In this study, we fabricated PICs with an initial polymer concentration of 1 mg mL^{-1} for all cases and a charge ratio under neutral conditions (anionic–cationic ratio = 1 : 1) (Scheme 1). All PIC samples were chemically crosslinked for biological evaluation. Crosslinking was performed using EDC to crosslink $–NH_2$ on a catiomer side chain and –COOH on an aniomer side chain to form an amide bond, which can increase particle robustness.[18] The resulting PICs were purified and subjected to a TNBS assay for crosslinking degree determination to obtain PICs with crosslinking degrees of 50% and 80%. The three different morphologies are listed in Table 2: vesicles, micelles from PEG_{2k}–PAsp and PEG_{2k}–PLL (2k-micelle), and micelles from PEG_{5k}–PAsp and homo–PLL (5k-micelle). The morphologies of the resulting particles were confirmed using TEM (Fig. S16, ESI†). Zeta potential measurements indicated that all PICs had almost neutral values.

Correlation between the physicochemical properties of PICs and their cellular internalisation

Effect of chain length mismatching. Harada and Kataoka reported that oppositely charged PEGylated polyions with similar chain lengths showed preferable interactions by forming a zipper-closing assembly and a well-ordered PEG–PIC interface.[38] However, this well-ordered arrangement might result in a less entropic state of the PIC domains, that is, less dynamic and frustrated (temporarily unpaired) states in the ionic residues compared with PICs obtained from unmatched chain lengths. To confirm the impact of chain length matching on the PIC internalisation, we fabricated fluorescent dye-labelled PIC vesicles with the crosslinking degree of 80% using combinations of matched and mismatched chain lengths (Table 2). The molar ratio of cationic–anionic residues was adjusted to 1 : 1; thus, the overall charges were assumed to be neutral regardless of the chain length. DLS measurement indicated that PIC vesicles had a monodisperse distribution (Fig. S23, ESI†). Their cellular internalisation was evaluated using HeLa cells (human cervical cancer cells) by two methods: microscopic imaging by CLSM to observe internalised particles and FCM quantification to quantify the total fluorescence of particles on the cell surface and inside cells.

Consequently, mismatched pairings of PEG–PAsp and homo–PLL with the DP (56, 100) and (93, 64), respectively, exhibited a higher cellular internalisation than matched pairing with the DP (69, 64) (Fig. 1). Furthermore, there was no significant difference between (56, 100) and (93, 64), indicating no preference for longer polymer charge signs. Notably, cellular internalisation was found to be similar for PIC (56, 100) and (93, 64), despite the difference in the weight fraction of PEG (f_{PEG}) values. In all cases, PICs were found inside the cells and were possibly internalised by endocytosis. Nevertheless, by the calcein leakage assay of PIC (56, 100), endosomal escape cannot

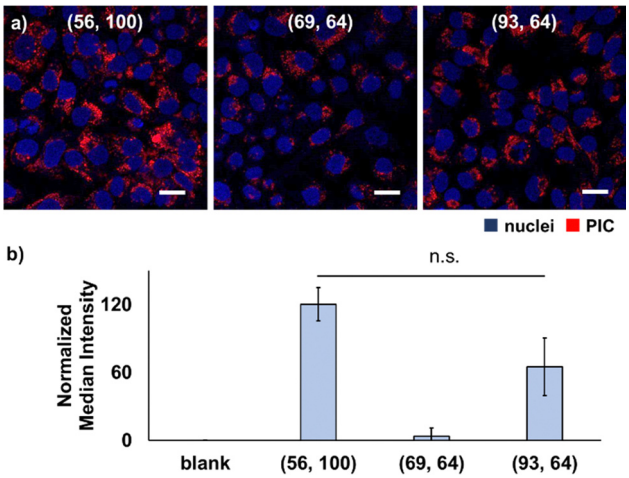

Fig. 1 Cellular internalisation of vesicles with different chain length combinations. (a) CLSM images of HeLa cells after 24-h incubation with the 80%-CL PIC with different chain length combinations. Blue, Hoechst 33342-(nuclei); red, Cy3-labelled PEG_{2k}-PAsp (PICs). (b) Fluorescence quantification of cells after 24 h-incubation detected by FCM (means ± standard deviation). Chain lengths are shown as (the DP of the aniomer, the DP of the catiomer).

be confirmed, which is supported by the overlapping fluorescence signal of calcein and PIC entrapped in endosomes (Fig. S25, ESI†). Overall, these results suggested that mismatched pairing in PICs can enhance their cellular internalisation. Presumably, this trend can be explained by the existence of dynamic and transient unpaired ionic residues, that is, a frustrated state in proximity to the interfacial region of the PIC domain and PEG palisades. Since the length of the polymer might contribute to cellular internalisation, that is, shorter chain lengths might suppress the internalisation to a certain extent, we focused on PICs with mismatched chain lengths with slightly shorter PAsp and longer PLL for further evaluation in the remainder of this study.

Effect of cationic residues on cellular internalization. The effect of residual side-chain properties was assessed using 50%-CL vesicles, in which cationic residues (primary amino groups) were modified by (1) acetylation or (2) guanidinylation. Acetylation can cap cationic charges with neutral functionalities. After acetylation, the resulting PIC exhibited a lower potential and a slightly larger particle size, which can be explained by the remaining anionic charges and further repulsion in the PIC domain (Table 2). Overall, all vesicles retained their morphology and distribution even after modification (Fig. S17 and S24, ESI†).

Next, to test the effect of another type of cationic residue and guanidium group, guanidinylation was performed on the primary amino groups of the catiomers. In previous reports, guanidinylation was performed against the catiomer before PIC formation, and the resulting PIC particles showed improved stability for the application.[33] However, direct comparison with regular PEG–PAsp/PLL PICsomes is difficult because the preparation conditions of guanidinylated polymer-based PICs were different from those of conventional PICsomes without

guanidinium functionalities. In this study, guanidinylation was conducted for ready-made PIC particles, which allowed us to use the same platform particles and evaluate the effect of ionic residues more directly. The introduction of guanidinium groups into the PIC domain resulted in the formation of slightly smaller particles with similar ζ-potentials, possibly because of the stronger binding of $-COO^-$ and $-NH\text{-}(C{=}NH_2^+)\text{-}NH_2$ *via* salt bridge formation (Table 2).

Both modifications resulted in the decreased cellular internalisation by HeLa cells after 24 h of incubation (Fig. 2a and d). Capped cationic residues may impede the interaction between the acetylated vesicles and the cell surface. In the case of guanidinylated vesicles, the introduction of a guanidium group inside the PIC domain enhances the interaction between the catiomer and aniomer, stabilising the PIC domain to exhibit less interaction with cells. Considering these results, the cell–PIC interaction was mainly ascribed to the interaction between dynamic cationic residues and certain cell surface components, presumably negatively charged components, *via* electrostatic interactions. In other words, the presence of negatively charged materials on the cell surface and positively charged materials with high mobility in the PIC domain is essential for particle recognition on the cell surface and further cellular internalisation. Therefore, the states of the PIC domain are considered to be recognisable by the cell surface, indicating that the modulation of the states of the PIC domain is a promising strategy for managing the interaction of nanoparticles with living cells.

Effect of cell-surface glycosaminoglycans (GAGs)-deficient proteoglycans on the cell–PIC interaction. In the previous section, we assumed that negatively charged cell-surface components played a crucial role. All eukaryotic cells contain negatively charged glycosaminoglycans (GAGs) as a part of proteoglycans on their cell surface. GAGs function as cell hydration agents, scaffolds, and facilitators of cell signalling processes such as cell growth and proliferation and cell adhesion.[39] Therefore, we decided to evaluate the effect of GAGs on the interaction of PICs with the cell surface. The 50%-CL vesicle was incubated with wild-type CHO-K1 cells (Chinese hamster ovary cells) or their genetic recombinant, CHO-A745 cells, which have a defect in xylosyltransferase, the enzyme that catalyses the first sugar transfer in GAG synthesis, and thus do not produce GAGs.[40] As shown in Fig. 2b, GAGs-deficient cells, CHO-A745, exhibited reduced vesicle internalisation after 24 h of incubation. This result supports the hypothesis that the presence of negatively charged GAGs on the cell surface is crucial for facilitating PIC interaction with the cell surface and further internalisation.

Effect of PIC crosslinking. In this study, all PICs were crosslinked for cell experiments. The crosslinking treatment is indispensable for increasing the stability of PIC vesicles for their application under physiological conditions.[31] Moreover, Mutaf *et al.* reported that crosslinking treatment was helpful in modulating the permeability of the PIC vesicle membrane *via* amide bond formation between a carboxylate group on the aniomer and a primary amine group on the catiomer.[32] As discussed in previous sections, cationic residues play a key role in cell interactions. We assumed that the degree of crosslinking affects cell internalisation and decided to investigate the correlation between the crosslinking degree, crosslinking-related physical properties (such as vesicle deformability) and cell internalisation.

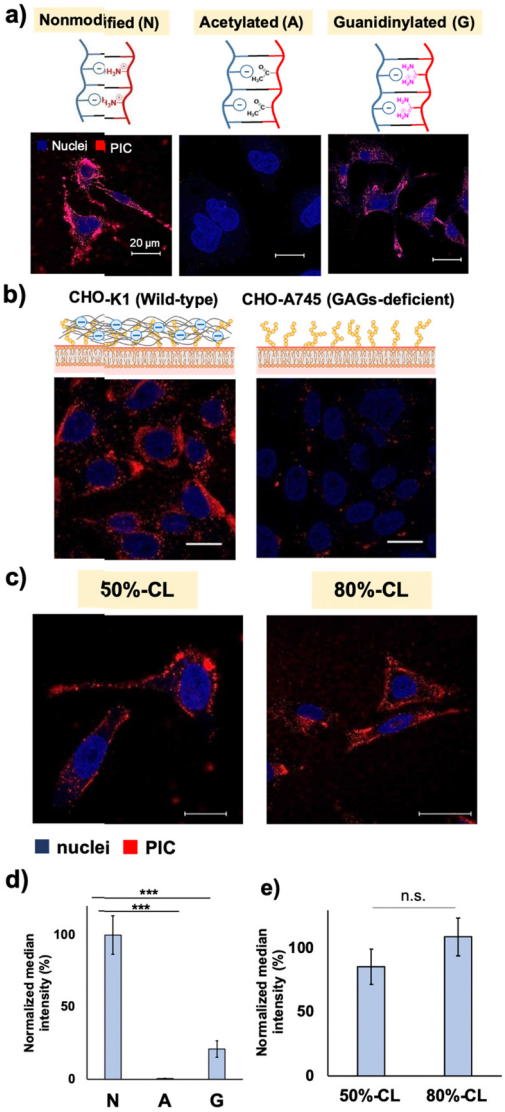

Fig. 2 Effect of the charge state difference on the cell–PIC interaction. (a) CLSM images of HeLa cells treated with non-modified (N), acetylated (A) and guanidinylated (G) PIC vesicles after 24 h of incubation. (b) CLSM images of the effect of cell-surface glycosaminoglycans (GAGs) on the cell–PIC interaction using wild-type CHO-K1 (left) and GAG-deficient CHO-A745 (right). Red, 50%-CL vesicle; blue, Hoechst-stained nuclei (scale bar: 20 μm). (c) Fluorescence microscopic evaluation of the crosslinking degree dependency of the cell–PIC interaction using 50%- and 80%-CL vesicles (scale bar: 20 μm). (d) Quantification results of cellular internalisation of non-modified/modified PICs by FCM (*y*-axis was normalised to the *N*-vesicle) and (e) that between 50%- and 80%-CL vesicles by FCM (*y*-axis was normalised to the 80%-CL vesicle).

First, the evaluation focused on vesicle deformability, which was expected to correlate with the degree of crosslinking owing to the restriction of polypeptide chain movement in the PIC domain. We estimated that the difference in deformability could be visualised using AFM, particularly by measuring the

vesicle-spreading area on the mica substrate. The vesicle spreading area can be interpreted as the contact area on the cell surface upon recognition by cells. A series of vesicles with different degrees of crosslinking, namely 50%- and 80%-CL, were prepared (Table 2). Notably, PIC vesicles with a crosslinking degree of $<50\%$ could be obtained; however, particle loss occurred during the purification process; this loss may be attributed to nonspecific adsorption onto the filtration membrane. In addition, vesicles without crosslinking were not prepared because non-crosslinked PICs are unstable and their behaviour is unpredictable. After the crosslinking treatment, the number of residual amine groups was determined using the TNBS assay to determine the degree of crosslinking of the particles (Scheme S1 and eqn (S2), ESI†). The degree of crosslinking was obtained from the remaining amine ratio, which was calculated using the amount of remaining amine in the complex quantified by TNBS assay using a calibration curve for PLL (Fig. S19 and S20, ESI†). The remaining amine ratio was calculated as the ratio of the amount of remaining amine and the total amount of amine existing before crosslinking, which was obtained from the amount of polyanions under the assumption of equimolar charge ratio in the PIC (see Fig. S21 and S22 for polymer calibration curves, ESI†).

AFM images showed higher deformability for 50%-CL vesicles than that for 80%-CL vesicles, based on information on the spreading area on the mica surface (Fig. 3). However, no significant difference was observed between the vesicles in terms of cellular internalisation (Fig. 2c and 2e). Thus, the difference in deformability in this range may not be significant for determining the difference in cellular internalisation. This result has several interpretations. First, vesicle–mica interaction and subsequent deformation of vesicles occur more explicitly under *in situ* conditions than under cell culture conditions, under which proteins and other biological components inhibit the effective interaction of PICs with the cell surface. Second, although the charge density of mica (0.02–0.5 $e^- nm^{-2}$, as reported by Pashley, 1981 and Israelachvili and Adams, 1978)[41,42] is comparable to that of the HeLa cell surface (-12 mC m^{-2}, which is equal to 0.072 $e^- nm^{-2}$),[43] the real cell surface is not as hard and flat as the mica surface. Specifically, the cells possess a three-dimensional proteoglycan structure that forces the PICs to behave differently. Finally, PICs with different deformabilities did not differ significantly in their interactions with the cell surface. Thus, in the present experimental design, such deformation of the cell surface was not the primary factor for the vesicles. Instead, dynamic cationic charges can be a dominant factor in cell–PIC interactions. In addition, PIC vesicles with 20–50% non-crosslinked cations exhibited similar interaction capabilities, regardless of the difference in the residual number of cationic charges in the PIC domain.

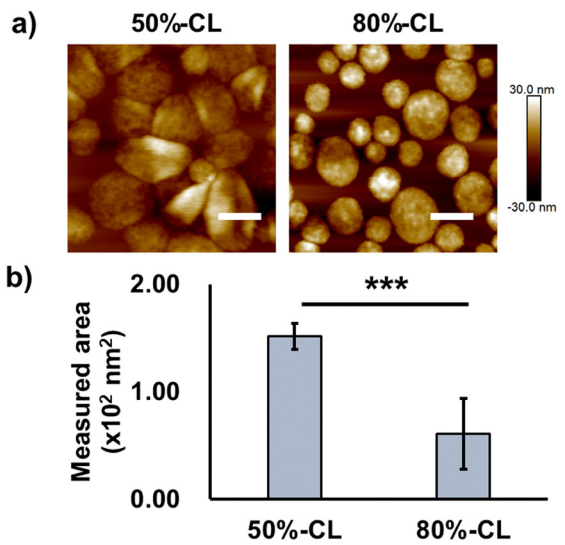

Fig. 3 Deformable properties of PIC vesicles with different crosslinking rates. (a) AFM results of vesicles with different crosslinking rates (scale bar: 200 nm) measured under wet conditions (PBS buffer) on the mica surface; (b) the area of particle deformation (analysed using ImageJ, quantified from a minimum of 20 particles and shown as means ± standard deviation).

Effect of morphologies and the PEG length. Established polymeric nanomaterials are classified into several morphologies, which may consequently influence their biological fate.[44] In the PIC system, PEG, a neutral block in a block copolymer, acts as a non-associative block in the whole assembly, which causes micro-segregation of the PIC domain and/or regulates the resulting structure of nano-assemblies. In general, the PEG weight fraction (f_{PEG}) of PIC-based assemblies is a useful indicator to predict and design their final morphologies.[17] Herein, two types of morphologies were selected for comparison: vesicles and micelles. PIC vesicles are characterised by their hollow structure formed *via* the enclosure of a PIC domain sandwiched between PEG palisades.[16] Meanwhile, PIC micelles are spherical particles consisting of a PIC core surrounded by a PEG shell (Fig. 4a).[11] In this study, both the vesicles and micelles were designed to have PEG chains of similar length, PEG_{2k}. From the CLSM observations, the PIC vesicles showed a more intense interaction with the cell surface and were more internalised by cells than the micelles (Fig. 4b, c and Fig. S26, ESI†).

The PIC domain structure and f_{PEG} may be key to determining the trend for the interaction with cells. While the PIC micelle possesses a core–shell structure with higher f_{PEG} ($\geq \sim 14\%$), the PIC vesicle has a hollow structure with lower f_{PEG} ($\leq \sim 10\%$), which can provide a more accessible two-dimensional lamellar structure of PIC with a large area at its interface against a PEG layer. The unilamellar structure of the PIC vesicle was confirmed by cryo-TEM (Fig. S18, ESI†). The thickness of the PIC membrane was estimated to be $\sim 12.0 \pm 2.5$ nm, which is close to the previously reported value.[16] Moreover, as shown in the AFM results, the hollow PIC architecture exhibited a deformable nature, which may result in a remarkable difference in the interaction with the cells. Presumably, the deformable vesicle architecture may promote the exposure of its PIC domain to the exterior, in contrast to the zero-dimensional architecture of the PIC micelle. However, we could not complete the deformability measurement of 2k-micelles owing to the less adherent properties of micelles on

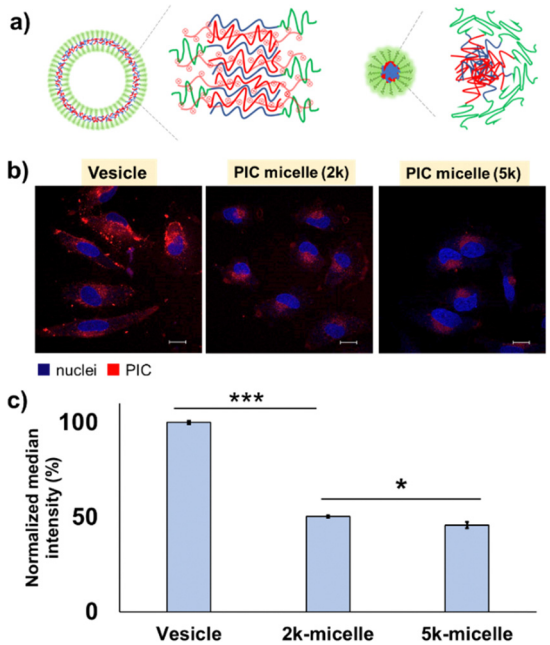

Fig. 4 Morphology dependency of the cell–PIC interaction. (a) Schematic illustration of the domain structure difference between vesicles (left) and micelles (right); (b) CLSM observation of PIC vesicles, 2k-micelles and 5k-micelles after 24 h of incubation with HeLa cells (scale bar: 20 μm; blue, Hoechst-stained nuclei; red, PIC); and (c) their quantification results after 24 h of incubation with HeLa cells by FCM (*y*-axis is normalised against vesicles).

the mica surface. This behaviour can be ascribed to the effective coverage of PEG chains on the rigid PIC core.

It is noteworthy that PIC vesicles formed aggregates on the surface of most cells (Fig. S26, ESI†), while less aggregate formation was observed for 2k- and 5k-micelles; in fact, 10% and 8% of the cells ($N \sim 100$) showed aggregate formation on their surface, respectively (data not shown). This indicates that the exposed PIC domains of vesicles may cause secondary aggregation on the cell surface, which can inhibit further cell internalization and show long-term retention on the cell surface. Besides domain structure and deformability, the size effect might play a certain role in cellular uptake. As an example of a similar trend, in the case of polystyrene nanoparticles, the highest cellular uptake efficiency is found for the particles with the size of 100 nm, while the particles with the size less than 50 nm exhibited less potency owing to a point at which the size no longer has a significant impact on cellular uptake.[45] Similar to this report, PIC vesicles with the size of 100–200 nm showed better internalisation than micelles with the size <50 nm, presumably owing to their higher surface area and deformable nature. However, further investigation is needed to prove this point.

In addition, to inspect the effect of PEG length, we used PICs with the same morphology and similar f_{PEG}. In fact, 2k- and 5k-micelles with close f_{PEG} values were selected for this purpose (Table 2). Due to similar f_{PEG} values, we expected that exposure of the PIC domain might be close. After 24 h of incubation with HeLa cells, the results showed that the 2k-micelle exhibited a slightly higher cellular internalisation than the 5k-micelle (Fig. 4c). Detailed analysis was performed using images obtained by CLSM (Fig. 4b and Fig. S27, ESI†). Results show that cellular internalisation is promoted for the 2k-micelle. This might be explained by the particle number. Probably, the greater number of particles in the 2k-micelle is due to its smaller particle size compared to that of the 5k-micelle, which increased the cell–PIC interaction probability. The subcellular distribution of PIC micelles seems similar, that is, most particles were found in the region between cell and nuclear membranes in a dot-like pattern, supported by the line profiling analysis (Fig. S27, ESI†). Presumably, all PIC micelles would be endocytosed and not escape from the endosome. At this stage, the difference in cellular uptake efficiency can also be explained by the longer PEG chain length for suppressing interaction with cells and higher f_{PEG} value. Nevertheless, the PEG chain length effect can be found to be the size and morphology determinant factor, which should be considered for the design of particles. Moreover, different subcellular distributions are confirmed for the PIC vesicles, in which vesicular PICs were more prominently found in the cell membrane region, indicating that PIC vesicles show higher cell surface adsorption and retention capability (Fig. S26 and S27, ESI†). This result seems consistent with the deformable nature of vesicles as discussed above. Thus, in terms of cellular uptake behaviour, the image-based analysis showed a similar trend to the FCM results, PIC vesicles $>$ 2k-micelles $>$ 5k-micelles. Overall, all PICs are considered to be endocytosed in HeLa cells judging from their size, $\leq$100 nm,[46] but further investigation is required.

Cell line dependency. To expand the potential utility as an *in vivo* delivery vehicle, we tested the cell line dependency of the PIC cellular internalisation using non-phagocytic and phagocytic cell lines. Particularly, HeLa and Caco2 (human colorectal adenocarcinoma), which are commonly used as epithelial cell models, and antigen-presenting immune cell lines (APCs), RAW 264.7 (mice macrophages) and DC 2.4 (mice dendritic cells), which have phagocytic activity, were chosen for this purpose. Generally, APCs can recognise foreign substances *via* specific receptors, that is, so-called pattern recognition receptors;[47] in this study, our particular interest is in scavenger receptors, which can effectively recognise negatively charged materials.[48] PIC vesicles with 50%-CL and its acetyl-modified variant were utilized for examining the cellular internalisation. The acetylated vesicles, which exhibited inadequate cell–PIC interactions with non-phagocytic cells HeLa and Caco-2, showed a clear interaction and internalisation by phagocytic cell lines (Fig. 5a and b). In particular, the macrophage cell line RAW 264.7 exhibited no significant change in the interaction between acetylated and non-modified vesicles. This is consistent with the capping of cationic groups and the subsequent charge repulsion of the remaining negative charges in the PIC domain. To confirm the possibility that scavenger receptors were involved in the internalisation of acetylated vesicles by RAW 264.7, dextran sulphate was added as a competitor to scavenger receptors, and internalisation was clearly inhibited

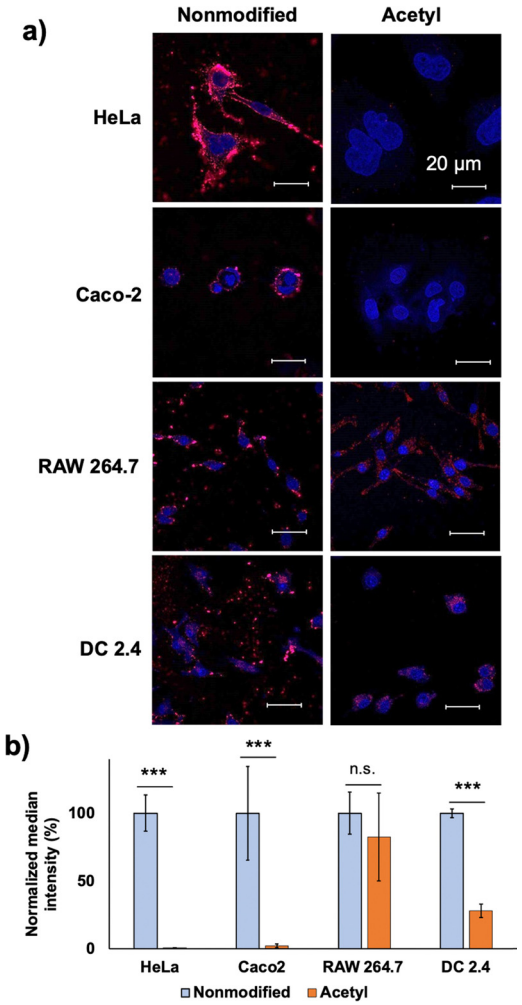

Fig. 5 Cell-line dependency of the cell–PIC interaction. (a) CLSM observations of 50% crosslinked vesicles with and without acetylation (scale bar: 200 nm; blue, Hoechst-stained nuclei; red, PIC) and (b) quantification by FCM. The *y*-axis was normalised against HeLa results.

(Fig. S28, ESI†). This finding also supports our hypothesis that the PIC domain can be recognised by the cell surface, and that modulation of the charged state can be an effective tool to change the fate of nanoparticles in physiological environments.

Cytotoxicity of PICs. Finally, the toxicity of PICs against the tested cell lines was evaluated using the component polymers, 50%-CL PICs, and modified vesicles. None of the PIC particles show significant toxicity in the tested cell lines after 24 h of incubation (Fig. S29, ESI†), indicating that PICs from the PEGylated polypeptides possess high biocompatibility.

Conclusion

In summary, we clarified several design aspects of PEGylated PICs to overcome the PEG dilemma by systematically tuning their properties; particularly, vesicle morphology with a mismatched catiomer–aniomer length enabled enhanced cell interaction capability. The PEG block length and crosslinking degree made a minor contribution to the cell–PIC interaction modulation. Remarkably, chemical modification of the PIC domain, particularly acetylation of the remaining amino groups, sharply inhibited the cell–PIC interaction with non-phagocytic cells, while retaining the interaction with phagocytic RAW264.7 cells. In the future, the insights of this study could be applied to the rational design of PEGylated PIC nanoparticles, where a balance between their stability, biocompatibility, and cellular internalisation can be achieved. Thus, our strategy is beneficial for the development of PEGylated nanocarriers without involving the PEG dilemma.

Author contributions

F. Aulia: conceptualisation, methodology, validation, investigation, writing – original draft, visualization; H.Matsuba: conceptualization, methodology, investigation, visualization; S. Adachi: methodology, investigation, visualization; T. Yamada: methodology, investigation, visualization; I. Nakase: cell line providence (CHO-A745), editing, validation; T. Nii: validation; T. Mori: validation; Y. Katayama: validation; and A. Kishimura: conceptualisation, methodology, investigation, writing – reviewing and editing, validation, project administration, funding acquisition.

Conflicts of interest

There are no conflicts to declare.

Acknowledgements

This research was supported in part by KAKENHI (Grant No. JP18H03534 and JP22H02202 (from JSPS) and JP22H05429 (from MEXT) to A. K.), and a Monbukagakusho Scholarship, MEXT (to F. A.). The authors are grateful to the Nanotechnology Platform Program and Advanced Research Infrastructure for Materials and Nanotechnology in Japan (ARIM) of MEXT of Kyushu University and the University of Tokyo for their valuable support with the TEM analysis. We thank Drs M. Tanaka, D. Murakami and S. Shiomoto (Kyushu University) for their assistance with the AFM measurements, as well as Drs M. Goto, N. Kamiya and R. Wakabayashi (Kyushu University) for their assistance with the CLSM measurements.

References

1 J. M. Harris and R. B. Chess, *Nat. Rev. Drug Discovery*, 2003, **2**, 214–221.
2 T. M. Allen, G. A. Austin, A. Chonn, L. Lin and K. C. Lee, *Biochim. Biophys. Acta*, 1991, **1061**, 56–64.
3 B. Pelaz, P. del Pino, P. Maffre, R. Hartmann, M. Gallego, S. Rivera-Fernández, J. M. de la Fuente, G. U. Nienhaus and W. J. Parak, *ACS Nano*, 2015, **9**(7), 6996–7008.
4 S. Mishra, P. Webster and M. E. Davis, *Eur. J. Cell Biol.*, 2004, **83**(3), 97–111.
5 H. Hatakeyama, H. Akita and H. Harashima, *Biol. Pharm. Bull.*, 2013, **36**(6), 892–899.

6 Y. Fang, J. Xue, S. Gao, A. L. D. Yand, H. Jiang, Y. He and K. Shi, *Drug Delivery*, 2017, **24**(2), 22–32.
7 E. Oh, J. B. Delehanty, K. E. Sapsford, K. Susumu, R. Goswami, J. B. Blanco-Canosa, P. E. Dawson, J. Granek, M. Shoff, Q. Zhang, P. L. Goering, A. Huston and I. L. Medintz, *ACS Nano*, 2011, **5**(8), 6434–6448.
8 Y. Li, M. Kröger and W. K. Liu, *Biomaterials*, 2014, **35**(30), 8467–8478.
9 A. Harada and K. Kataoka, *Macromolecules*, 1995, **28**, 5294–5299.
10 H. Cabral, K. Miyata, K. Osada and K. Kataoka, *Chem. Rev.*, 2018, **118**(14), 6844–6892.
11 J. Sun and Z. Li, *Macromolecules*, 2020, **53**(20), 8737–8740.
12 K. Itaka, K. Yamauchi, A. Harada, K. Nakamura, K. H. Kawaguchi and K. Kataoka, *Biomaterials*, 2003, **24**(34), 4495–4506.
13 K. Kataoka, H. Togawa, A. Harada, K. Yasugi, T. Matsumoto and S. Katayose, *Macromolecules*, 1996, **29**(26), 8556–8557.
14 A. Harada and K. Kataoka, *Macromolecules*, 1998, **31**(2), 288–294.
15 L. Zhao, M. Skwarczynski and I. Toth, *ACS Biomater. Sci. Eng.*, 2019, **5**(10), 4937–4950.
16 Y. Anraku, A. Kishimura, M. Oba, Y. Yamasaki and K. Kataoka, *J. Am. Chem. Soc.*, 2010, **132**, 1631–1636.
17 S. Chuanoi, A. Kishimura, W. Dong, Y. Anraku, Y. Yamasaki and K. Kataoka, *Polym. J.*, 2014, **46**(7), 130–135.
18 W. Dong, A. Kishimura, Y. Anraku, S. Chuanoi and K. Kataoka, *J. Am. Chem. Soc.*, 2009, **131**, 3804–3805.
19 A. Ahmad, T. Nii, T. Mori, Y. Katayama, M. Toyofuku and A. Kishimura, *Macromol. Rapid Commun.*, 2022, 2200316.
20 K. Naoyama, K. T. Mori, Y. Katayama and A. Kishimura, *Macromol. Rapid Commun.*, 2016, **37**, 1087–1093.
21 A. Koide, A. Kishimura, K. Osada, W. D. Jang, Y. Yamasaki and K. Kataoka, *J. Am. Chem. Soc.*, 2006, **128**(18), 5988–5989.
22 Y. Anraku, A. Kishimura, M. Kamiya, S. Tanaka, T. Nomoto, K. Toh, Y. Matsumoto, S. Fukushima, D. Sueyoshi, M. R. Kano, Y. Urano, N. Nishiyama and K. Kataoka, *Angew. Chem., Int. Ed.*, 2016, **55**, 560–565.
23 D. Sueyoshi, Y. Anraku, T. Komatsu, Y. Urano and K. Kataoka, *Biomacromolecules*, 2017, **18**(4), 1189–1196.
24 D. Kokuryo, Y. Anraku, A. Kishimura, S. Tanaka, M. R. Kano, J. Kershaw, N. Nishiyama, T. Saga, I. Aoki and K. Kataoka, *J. Controlled Release*, 2013, **169**, 220–227.
25 W. Kawamura, Y. Miura, D. Kokuryo, K. Toh, N. Yamada, T. Nomoto, Y. Matsumoto, D. Sueyoshi, X. Liu, I. Aoki, M. R. Kano, N. Nishiyama, T. Saga, A. Kishimura and K. Kataoka, *Sci. Technol. Adv. Mater.*, 2015, **16**, 035004.
26 B. S. Kim, S. Chuanoi, T. Suma, Y. Anraku, K. Hayashi, M. Naito, H. J. Kim, I. C. Kwon, K. Miyata, A. Kishimura and K. Kataoka, *J. Am. Chem. Soc.*, 2019, **141**(8), 3699–3709.
27 B. S. Kim, M. Naito, H. Chaya, M. Hori, K. Hayashi, H. S. Min, Y. Yi, H. J. Kim, T. Nagata, Y. Anraku, A. Kishimura, K. Kataoka and K. Miyata, *Biomacromolecules*, 2020, **21**(10), 4365–4376.
28 S. Chuanoi, Y. Anraku, M. Hori, A. Kishimura and K. Kataoka, *Biomacromolecules*, 2014, **15**(7), 2389–2397.
29 A. Goto, H. Yen, Y. Anraku, S. Fukushima, P. Lai, M. Kato, A. Kishimura and K. Kataoka, *ACS Biomater. Sci. Eng.*, 2017, **3**(5), 807–815.
30 A. Goto, Y. Anraku, S. Fukushima and A. Kishimura, *Polymers*, 2023, **15**, 1368.
31 Y. Anraku, A. Kishimura, A. Kobayashi, M. Oba and K. Kataoka, *Chem. Commun.*, 2011, **47**, 6054–6056.
32 O. F. Mutaf, Y. Anraku, A. Kishimura and K. Kataoka, *Polymer*, 2017, **133**, 1–7.
33 M. Hori, H. Cabral, K. Toh, A. Kishimura and K. Kataoka, *Biomacromolecules*, 2018, **19**, 4113–4121.
34 M. Nakanishi, J. S. Park, W. D. Jang, M. Oba and K. Kataoka, *React. Funct. Polym.*, 2007, **67**, 1361–1372.
35 Y. Liu, T. Maruyama, B. KC, T. Mori, Y. Katayama and A. Kishimura, *Chem. Lett.*, 2021, **50**, 1034–1037.
36 O. F. Mutaf, A. Kishimura, Y. Mochida, A. Kim and A. K. Kataoka, *Macromol. Rapid Commun.*, 2015, **36**, 1958–1964.
37 A. Carlsen and S. Lecommandoux, *Curr. Opin. Colloid Interface Sci.*, 2009, **14**, 329–339.
38 A. Harada and K. Kataoka, *Science*, 1999, **283**(5398), 65–67.
39 R. Raman, V. Sasisekharahn and R. Sasisekharan, *Chem. Biol.*, 2005, **12**(3), 267–277.
40 J. D. Esko, T. E. Stewart and W. H. Taylor, *Proc. Natl. Acad. Sci. U. S. A.*, 1985, **82**(10), 3197–3201.
41 R. M. Pashley, *J. Colloid Interface Sci.*, 1981, **80**(1), 153–162.
42 J. N. Israelachvili and G. E. Adams, *J. Chem. Soc., Faraday Trans. 1*, 1978, **74**, 975–1001.
43 L. Ouyang, R. Shaik, R. Xu, G. Zhang and J. Zhe, *Cells*, 2021, **10**(6), 1519.
44 F. Alexis, E. Pridgen, L. K. Molnar and O. C. Farokhzad, *Mol. Pharmaceutics*, 2008, **5**(4), 505–515.
45 K. Y. Win and S. S. Feng, *Biomaterials*, 2005, **26**(15), 2713–2722.
46 J. Rejman, V. Oberle, I. S. Zuhorn and D. Hoekstra, *Biochem. J.*, 2004, **377**(1), 159–169.
47 S. Gordon, *Cell*, 2002, **111**, 927–930.
48 E. Fröhlich, *Int. J. Nanomed.*, 2012, **7**, 5577–5591.

